

# SIMULATING EARTHQUAKE-INDUCED SLOPE FAILURES USING A SOLID-FLUID COUPLING MODEL BASED ON THE SMOOTHED PARTICLE HYDRODYNAMICS FRAMEWORK

\*Yusuke Ono<sup>1</sup>

<sup>1</sup>Faculty of Engineering, Tottori University, Japan

\*Corresponding Author, Received: 30 Nov. 2020, Revised: 04 Feb. 2021, Accepted: 23 Feb. 2021

**ABSTRACT:** Various numerical analysis methods have been developed to simulate earthquake-induced slope failures. Simulations of earthquake-induced slope failures require capabilities to reproduce some factors, including the trigger level of an input ground motion and a travel distance of debris. For reproducing a trigger level of an input motion, the finite element method based on solid mechanics has been used. For reproducing a travel distance of debris, simulation methods based on the fluid dynamics have been applied. This study presents a new approach to simulate an earthquake-induced slope failure, coupling the solid mechanics and the fluid dynamics, based on the framework of the smoothed particle hydrodynamics (SPH). The presented approach allows us to simulate an earthquake-induced slope failure from its triggering stage to its accumulation stage. The presented approach demonstrated its capabilities to reproduce the trigger level of ground motion and a travel distance of debris through several simulation cases. The paper concluded that the presented approach could be a promising method to simulate earthquake-induced slope failures.

*Keywords:* Earthquake-induced slope failure, Smoothed particle hydrodynamics, Earthquake response, Run-out

## 1. INTRODUCTION

Once a strong earthquake strikes a mountainous area, slope failures, landslides, and rockfalls are likely to occur [1]. The 1994 Northridge earthquake (Mw 6.7) triggered more than 11,000 slope failures that killed 61 people [2]. The 2004 Chuetsu earthquake (Mw 6.6) induced about 9200 slope failures, and 68 people lost their lives [3]. More than 200,000 slope failures were caused by the 2008 Wenchuan earthquake (Mw 7.9) and resulted in 87,633 casualties [4].

Numerical simulation techniques have been developed to reproduce an earthquake-induced slope failure. The sliding block model is used to examine the occurrence possibility of slope failure for a certain level of earthquake excitation [5]. The finite element (FE) analysis can be used to investigate slope stability more precisely than the analysis using the sliding block model [6]. Typically, a slope is modeled by an elastic or an elastoplastic solid material in the FE analysis. However, the FE analysis has difficulties in simulating a flow-like slope failure.

For simulating a flow-like slope failure, the smoothed particle hydrodynamics (SPH) method has been applied recently. The SPH method was initially invented in the field of astrophysics [7]. Afterward, the application of the SPH method has extended to fluid dynamics and solid dynamics. A slope failure occurred in the municipal solid waste was simulated by the SPH with a Bingham fluid

model [8]. The SPH with a Bingham fluid model was also applied to earthquake-induced landslides [9-11]. These studies report that the SPH with a Bingham fluid model can reproduce surface profile of post-failure and run-out distance.

The aim of this paper is to develop a coupling model of solid and fluid dynamics into the SPH framework for simulating an earthquake-induced slope failure or landslide. The developed model is expected to simulate an entire process of an earthquake-induced slope failure: response to an earthquake ground motion, occurrence of flow sliding, and accumulation of debris.

## 2. SIMULATION MODEL

First, the framework of the SPH method is introduced. Second, the SPH discretization of equations of motion is given for a solid body and a fluid, respectively. Third, a new coupling model of solid-fluid dynamics is proposed.

### 2.1 SPH Framework

The SPH framework consists of two fundamental approximation techniques: kernel approximation, and particle approximation. The kernel approximation is based on the following identical equation:

$$f(\mathbf{x}) = \int_D f(\mathbf{x}') \delta(\mathbf{x} - \mathbf{x}', h) d\mathbf{x}' \quad (1)$$

where  $f(\mathbf{x})$  is a function of the position vector  $\mathbf{x}$ ;  $\delta(\mathbf{x})$  is the Dirac delta function;  $D$  is the problem domain. The kernel approximation in the SPH is defined by replacing  $\delta(\mathbf{x})$  by a smoothing kernel function  $W(\mathbf{x})$ :

$$f(\mathbf{x}) \approx \int_D f(\mathbf{x}') W(\mathbf{x} - \mathbf{x}', h) d\mathbf{x} \quad (2)$$

where  $h$  is called the smoothing length that prescribes the width of the function. A smoothing kernel function  $W(\mathbf{x})$  must be a differentiable even function and must satisfy with the following conditions:

$$\int_D W(x, h) dx = 1 \quad (3)$$

$$\lim_{h \rightarrow 0} W(x, h) = \delta(x) \quad (4)$$

The particle approximation is introduced by the discretized form of Eq. (2) as follows:

$$f(x_i) \approx \sum_{j=1}^N m_j \frac{f(x_j)}{\rho_j} W(x_i - x_j, h) \quad (5)$$

where  $m_j$  denotes the mass of particle  $j$ .

## 2.2 Equation of Motion

The equation of motion of a solid body or a fluid is given by,

$$\frac{dv^\alpha}{dt} = \frac{1}{\rho} \frac{\partial \sigma^{\alpha\beta}}{\partial x^\beta} + b^\alpha \quad (6)$$

where  $\alpha$  and  $\beta$  denote the coordinate directions;  $x^\alpha$  is the position vector;  $v^\alpha$  is the velocity vector;  $t$  is time;  $\rho$  is density;  $\sigma^{\alpha\beta}$  is the stress tensor;  $b^\alpha$  is the body force. The SPH form of the equation of motion is given by,

$$\frac{dv_i^\alpha}{dt} = \sum_{j=1}^N m_j \left[ \frac{\sigma_i^{\alpha\beta}}{\rho_i^2} + \frac{\sigma_j^{\alpha\beta}}{\rho_j^2} \right] \frac{\partial W_{ij}}{\partial x_j^\beta} + b_i^\alpha \quad (7)$$

## 2.3 Solid-fluid Coupling Model

In the present study, we propose that the stress tensor for a particle is computed by coupling solid and fluid states as follows:

$$\sigma^{\alpha\beta} = \beta(t)(\sigma^{\alpha\beta})^s + \{1 - \beta(t)\}(\sigma^{\alpha\beta})^f \quad (8)$$

where the superscript s and f denote solid and fluid

state, respectively;  $\beta(t)$  is a weight function for coupling the stresses of solid and fluid states and is defined by

$$\beta(t) = \exp\{-\gamma(t_f - t)\} \quad (9)$$

where  $\gamma$  is a coupling control parameter;  $t_f$  is the time when the stress tensor reaches the failure surface first time. For solid-state of a particle, the stress tensor  $(\sigma^{\alpha\beta})^s$  is calculated by the elastic constitutive model,

$$(\sigma^{\alpha\beta})^s = -p\delta^{\alpha\beta} + 2G\varepsilon^{\alpha\beta} \quad (10)$$

where  $p$  is the isotropic pressure;  $\delta^{\alpha\beta}$  is the Kronecker delta;  $G$  is the shear modulus;  $\varepsilon^{\alpha\beta}$  is the strain tensor. The isotropic pressure ( $p$ ) is calculated by

$$p = K\varepsilon^{\alpha\beta} \quad (11)$$

where  $K$  is the elastic bulk modulus.

On the other hand, the Bingham fluid model is applied to calculate the stress tensor of fluid-state. The stress tensor of fluid-state  $(\sigma^{\alpha\beta})^f$  is written by

$$(\sigma^{\alpha\beta})^f = -p\delta^{\alpha\beta} + \tau^{\alpha\beta} \quad (12)$$

where  $\tau^{\alpha\beta}$  is the shear stress tensor and is given by,

$$\tau^{\alpha\beta} = \eta\dot{\varepsilon}^{\alpha\beta} + \tau_y \quad (13)$$

where  $\eta$  is the viscosity coefficient;  $\dot{\varepsilon}^{\alpha\beta}$  is the strain rate tensor;  $\tau_y$  is the yield shear stress. To compute the isotropic pressure  $p$  of fluid, Eq. (11) is also applied.

The Mohr-Coulomb failure criterion is applied for both solid and fluid states of a particle. Furthermore, the strength reduction factor  $S_R$  is introduced. The relations between the internal friction angle of solid-state  $\phi_s$  and that of fluid state  $\phi_f$  is defined by

$$\phi_f = S_R\phi_s \quad (14)$$

The same  $S_R$  is used for the cohesion:

$$c_f = S_Rc_s \quad (15)$$

where  $c_s$  is the cohesion of solid-state of a particle;  $c_f$  is the cohesion of fluid-state.

## 2.4 Boundary Condition

The dynamic boundary condition is applied to

model the rigid box in the simulation. The positions of the boundary particles are fixed, while the same procedure as for the other particles computes the stress tensors of the boundary particles.

### 2.5 Rayleigh Damping

For stabilizing a simulation and absorbing the vibration of a model, Rayleigh damping is applied in this study. Rayleigh damping is commonly used in earthquake engineering. The application of Rayleigh damping to the SPH framework is appeared in the reference [13].

### 2.6 Time Integration

The Verlet time integration scheme is used to update the velocities and the positions of the particles, and the fixed time increment of  $1.0 \times 10^{-4}$  s is applied.

## 3. NUMERICAL EXAMPLE

A slope model is considered as an example to demonstrate the performance of the developed coupling model. The properties of the example slope model and other parameters required to execute the simulation is presented in this chapter.

### 3.1 Slope Model

The geometry of the example slope model is shown in Fig. 1. The slope angle of the model is  $60^\circ$ . The material properties for solid and fluid states of the slope are listed in Tables 1 and 2.

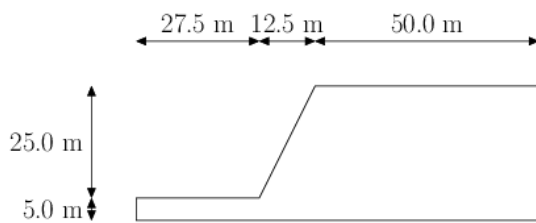


Fig. 1 The geometry of the slope model.

Table 1 Material properties for solid-state

Property	Value (Unit)
Density ( $\rho^s$ )	$1.964 \times 10^3$ (kg/m <sup>3</sup> )
Young's modulus ( $E$ )	$1.675 \times 10^6$ (kPa)
Poisson's ratio ( $\nu$ )	0.346
Cohesion ( $c^s$ )	150.0 (kPa)
Internal friction angle ( $\phi^s$ )	20.0 ( $^\circ$ )

Table 2 Material properties for fluid-state

Property	Value (Unit)
Density ( $\rho^f$ )	$1.964 \times 10^3$ (kg/m <sup>3</sup> )
Viscosity coefficient ( $\eta$ )	2.00 (Pa·s)
Cohesion ( $c^f$ )	$150.0S_R$ (kPa)
Internal friction angle ( $\phi^f$ )	$20.0S_R$ ( $^\circ$ )

Note:  $S_R$  denotes strength reduction factor

### 3.2 Input Ground Motion

The sinusoidal wave of the amplitude with 6.0 m/s/s is used as the horizontal ground motion (Fig. 2). For the vertical direction, the gravity load is applied. From  $t=0$  to 3 (s), no horizontal excitation is applied to stabilize the slope model to the gravity. The horizontal excitation starts at  $t=3$  (s), and its amplitude increases gradually. From  $t=9$  (s), the amplitude decreases and becomes zero at  $t=10$  (s).

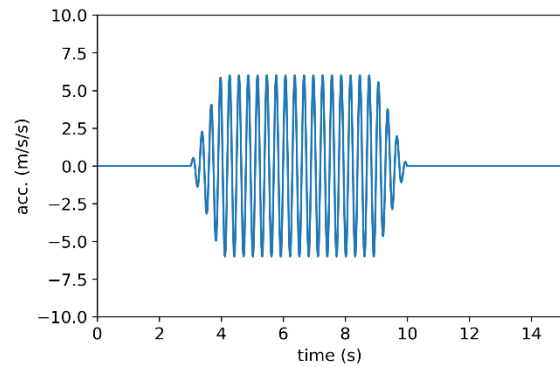


Fig. 2 The time history of the input acceleration.

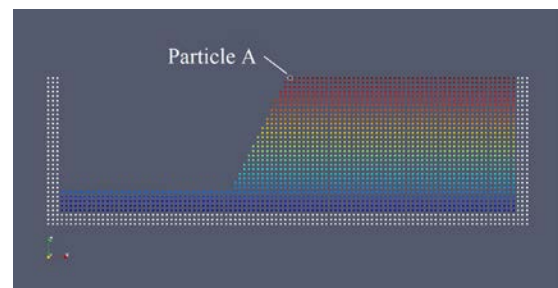
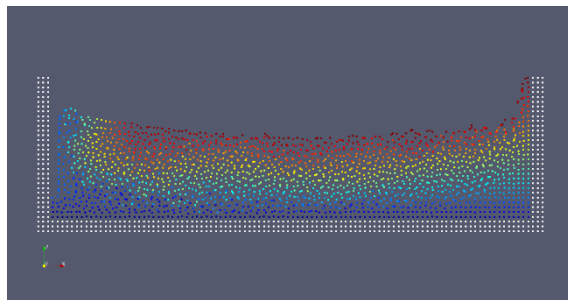


Fig. 3 The initial arrangement of particles.

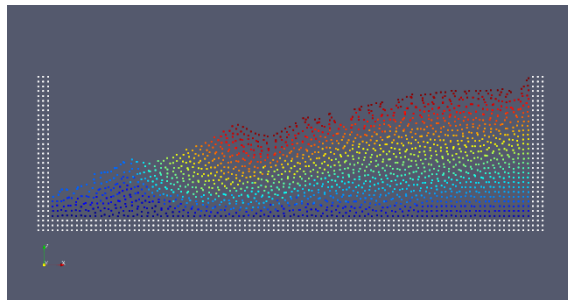
## 4. RESULTS

Figure 3 shows the initial configuration of the particles. The particles are placed homogeneously with 1.0 m intervals. The cubic spline type kernel function is used, and its smoothing length of the kernel function is 2.3 m. In total, 2,404 particles are used, including the boundary particles. The colors of the particles show their vertical positions, except the boundary particles colored in white.

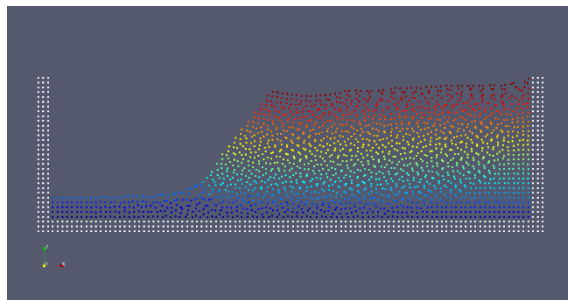
Figure 4 compares the profiles of the slope model after the horizontal excitation at  $t=15$  (s) for various strength reduction factors: (a)  $S_R=0.10$ ; (b)  $S_R=0.25$ ; (c)  $S_R=0.50$ . The colors indicate the initial height of the particles, except the boundary particles that are colored in white. The same color-coding is commonly used in Fig. 6. The coupling parameter ( $\gamma$ ) is 100.0. From these results, the effect of the strength reduction factor is revealed. The smaller value of  $S_R$  facilitates the deformation of the slope. For the case of  $S_R=0.10$ , the slope model is fluidized and deforms significantly. For the case of  $S_R=0.5$ , the slope model is not fluidized, although it deforms slightly.



(a)  $S_R=0.10, \gamma=100.0$



(b)  $S_R=0.25, \gamma=100.0$

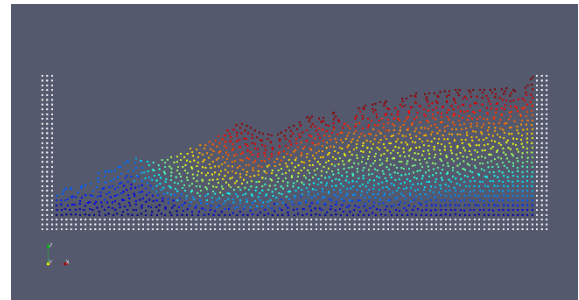


(c)  $S_R=0.50, \gamma=100.0$

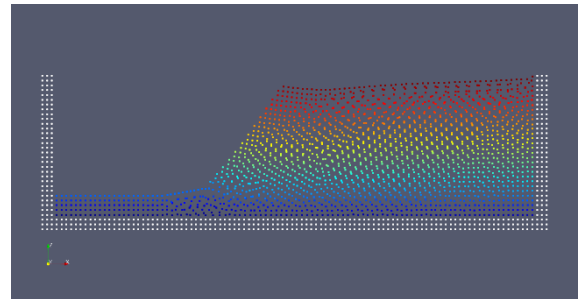
Fig. 4 Slope profiles after the horizontal excitation for  $S_R=0.10, 0.25$ , and  $0.50$ .

On the other hand, Fig. 5 compares the results for (a)  $\gamma=100.0$  and (b)  $\gamma=1.0$ . The strength reduction factor ( $S_R$ ) is the same and is 0.25. The result suggests that the larger value of the coupling parameter  $\gamma$  makes the slope model stable. For the larger value of the coupling parameter  $\gamma=100.0$ , the

slope model collapses, while it deforms slightly for the smaller value of  $\gamma=1.0$ .



(a)  $S_R=0.25, \gamma=100.0$



(b)  $S_R=0.25, \gamma=1.0$

Fig. 5 Slope profiles after the horizontal excitation at  $t=15$  (s) for  $\gamma=100.0$  and  $1.0$ .

Figure 6 compares the vertical motion of particle A, which is indicated in Fig. 2, for  $S_R=0.10, 0.25$ , and  $0.50$ . The effective time range of the horizontal ground motion is indicated in the figure. The moment when particle A starts moving is the same for all cases. For  $S_R=0.10$ , the slope model fluidizes, and particle A starts moving earlier than for the other cases. For  $S_R=0.50$ , the slope model fluidizes gradually, and the particle moves slowly. For  $S_R=0.50$ , the behavior of the slope model is intermediate of the other two cases.

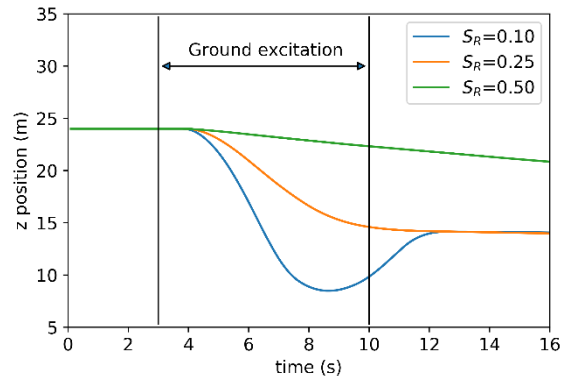


Fig. 6 The vertical displacement of particle A for  $S_R=0.10, 0.25$ , and  $0.50$  ( $\gamma=100.0$ ).

The vertical motions of particle A for  $S_R=0.25$ ,  $\gamma=100.0$  and  $1.0$  are compared in Fig.7. The coupling parameter ( $\gamma$ ) has the effect of delaying fluidization. For the case of  $\gamma=1.0$ , the slope model deforms gradually after the horizontal excitation ends. For  $\gamma=100.0$ , the deformation of the slope model begins and finishes during the horizontal excitation.

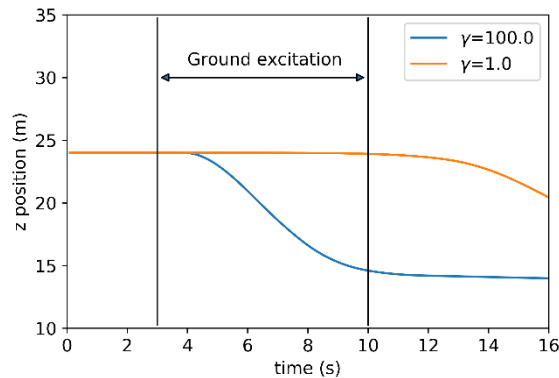


Fig. 7 The vertical displacement of particle A for  $\gamma=100.0$  and  $1.0$  ( $S_R=0.35$ ).

## 5. DISCUSSION AND CONCLUSION

In the application of the SPH method to earthquake-induced slope failures and landslides [8]–[11], fluid models such as Bingham fluid are commonly used to reproduce the fluidization and deposition process. In these studies, the occurrence process of a slope failure has been ignored. On the other hand, previous studies [12]–[15] attempted to simulate all processes of a slope failure or a landslide: occurrence, fluidization, and deposition. However, their studies are based on solid mechanics and have not adequately reproduced fluidization and decomposition processes.

In this study, we have developed a model coupling solid and fluid models. The developed model allows us to simulate the whole process of an earthquake-induced slope failure or landslide: the occurrence of failure, fluidization, and sedimentation. As a further study, an appropriate method for setting the simulation parameters corresponding to the material properties must be developed.

## 6. ACKNOWLEDGMENTS

This work was supported by JSPS KAKENHI Grant Number 18H01523.

## 7. REFERENCES

[1] Keefer D. K., Landslides caused by earthquakes,

Geological Society of America Bulletin, Vol. 95, pp.406–421, 1984.

- [2] Harp E.L. and Jibson R.W., Landslides triggered by the 1994 Northridge, California, earthquake, Bull. Seismol. Soc. Am., Vol. 86, pp. S319–S332, 1996.
- [3] Sekiguchi H. and Sato H., Feature and distribution of landslides induced by the Mid Niigata Prefecture earthquake in 2004, Japan, Landslides, Vol. 43, pp.142–154, 2006.
- [4] Dai F. C., Xu C., Yao X., Xu L., Tu X. B., and Gong Q. M., Spatial distribution of landslides triggered by the 2008 Ms 8.0 Wenchuan earthquake, China, J. of Asian Earth Sci., Vol. 40, pp.883–895, 2011.
- [5] Jibson R. W., Predicting earthquake-induced landslide displacements using Newmark’s sliding block analysis, Transportation Research Record, Vol. 1411, pp.9–17, 1993.
- [6] Toki K., Miura F., and Oguni, Y., Dynamic slope stability analysis with a non-linear finite element method, Earthquake Engineering & Structural Dynamics, Vol. 13, Issue 2, pp. 151–171, 1985.
- [7] Gingold R. A. and Monaghan J.J., Smoothed particle hydrodynamics: Theory and application to non-spherical stars, Monthly Notices of the Royal Astronomical, Vol. 181, pp.375–389, 1977.
- [8] Huang Y., Dai Z. L., Zhang W. J., and Huang M.S., SPH-based numerical simulations of flow slides in municipal solid waste landfills, Waste Management and Research, Vol. 31, Issue 3, pp.256–264, 2013.
- [9] Huang Y., Dai Z., Zhang W., and Chen Z., Visual simulation of landslide fluidized movement based on smoothed particle hydrodynamics, Natural Hazards, Vol. 59, Issue 3, pp.1225–1238, 2011.
- [10] Dai Z., Huang H., Cheng H., and Xu Q., 3D numerical modeling using smoothed particle hydrodynamics of flow-like landslide propagation triggered by the 2008 Wenchuan earthquake, Engineering Geology, Vol. 180, pp. 21–33, 2014.
- [11] Dai Z., Wang F., Huang Y., Song K., and Iio A., SPH-based numerical modeling for the post-failure behavior of the landslides triggered by the 2016 Kumamoto earthquake, Geoenvironmental Disasters, Vol. 3, 2016.
- [12] Ono Y., Nishida S., and Kiyono J., SPH Simulation for Seismic Behavior of Earth Structures, Proc. of 14<sup>th</sup> World Conference on Earthquake Engineering, Paper No.14-0145, 2008.
- [13] Ono Y., SPH Simulation of Earthquake-induced Slope Failure, Proc. of 15<sup>th</sup> World Conference on Earthquake Engineering, Paper No.22185, 2012.

- [14] Bui H.H. and Fukagawa R., An improved SPH method for saturated soils and its application to investigate the mechanisms of embankment failure: Case of hydrostatic pore-water pressure, *International Journal for Numerical and Analytical Methods in Geomechanics*, Vol.37, pp.31–50, 2013..
- [15] Chen W. and Qiu T., Simulation of earthquake-induced slope deformation using SPH method,

*International Journal for Numerical and Analytical Methods in Geomechanics*, Vol.38, Issue 3, pp.297–330, 2014.

---

Copyright © Int. J. of GEOMATE. All rights reserved, including the making of copies unless permission is obtained from the copyright proprietors.

---